PAPER

Check for updates

Selenium nanoparticle-functionalized injectable chitosan/collagen hydrogels as a novel therapeutic strategy to enhance stem cell osteoblastic differentiation for bone regeneration

Khaled Alajmi,†[ab] Matthew Hartford,†[ab] Nakka Sharmila Roy,[c] Anamitra Bhattacharya,[c] Santanu Kaity, [ID][c] Brenton L. Cavanagh,[d] Subhadeep Roy [ID] *[c] and Kulwinder Kaur*[ab]

Stem cells are an essential consideration in the fields of tissue engineering and regenerative medicine. Understanding how nanoengineered biomaterials and mesenchymal stem cells (MSCs) interact is crucial for their role in bone regeneration. Taking advantage of the structural stability of selenium nanoparticles (Se-NPs) and biological properties of natural polymers, Se-NPs-functionalized, injectable, thermoresponsive hydrogels with an interconnected molecular structure were prepared to identify their role in the osteogenic differentiation of different types of mesenchymal stem cells. Further, comprehensive characterization of their structural and biological properties was performed. The results showed that the hydrogels undergo a sol to gel transition with the help of β-glycerophosphate, while functionalization with Se-NPs significantly enhances their biological response through stabilizing their polymeric structure by forming Se–O covalent bonds. Further results suggest that Se-NPs enhance the differentiation of MSCs toward osteogenic lineage in both the 2D as well as 3D. We demonstrated that the Se-NPs-functionalized hydrogels could enhance the differentiation of osteoporotic bone-derived MSCs. We also focused on specific cell surface marker expression (CD105, CD90, CD73, CD45, CD34) based on the exposure of healthy rats' bone marrow-derived stem cells (BMSCs) to the Se-NP-functionalized hydrogels. This study provides essential evidence for pre-clinical/clinical applications, highlighting the potential of the nanoengineered biocompatible elastic hydrogels for bone regeneration in diseased bone.

1. Introduction

Hydrogels are highly hydrophilic, soft, three-dimensional (3D) networks that support cell attachment and proliferation.[1–3] Thermoresponsive hydrogels, or thermogels, transition from sol to gel with temperature changes without any toxic chemistry crosslinking,[4,5] making them ideal for delivering therapeutic cargos, like nanoparticles and drugs. These hydrogels can improve patient compliance *via* offering minimally invasive treatment, reduced side effects, and enhanced cargo activity.[6,7]

They have been widely used in cartilage, bone, and cardiac tissue engineering,[4,5] and can be prepared from different types of natural or synthetic polymers.

The natural polymer chitosan (CS) is an ideal material for the preparation of thermogels due to its biocompatibility and non-toxicity, favoring its use for bone tissue regeneration and controlled cargo delivery.[8–10] It was reported that CS solution gelled at 37 °C with the addition of the crosslinker β-glycerophosphate (β-GP) through hydrogen bonding and hydrophobic interaction.[10] However, while pure CS hydrogels have many advantages, their mechanical strength and degradation rate do not align well with the acidic environments found in diseased bone.[11–13] Combining CS with polymers, like collagen, or inorganic materials, like hydroxyapatite, can enhance their properties, making them suitable for bone tissue engineering.[14,15] Type I collagen (Coll) is a major component of the extracellular matrix in natural bone tissue that shows biocompatibility, biodegradability, non-toxicity, osteogenic induction properties, and low immunogenicity.[9] Pablo *et al.*16 reported CS/Coll hydrogels with superior thermomechanical and biocompatibility properties.

a School of Pharmacy & Biomolecular Sciences, Royal College of Surgeons (RCSI), Dublin D02YN77, Ireland. E-mail: KulwinderKaur@rcsi.com

b Tissue Engineering Research Group, Department of Anatomy & Regenerative Medicine, Royal College of Surgeons (RCSI), Dublin D02YN77, Ireland

c Department of Pharmacology and Toxicology, National Institute of Pharmaceutical Education and Research, Kolkata, West Bengal 700054, India. E-mail: subhadeep@niperkolkata.ac.in

d Cellular and Molecular Imaging Core, Royal College of Surgeons in Ireland, Dublin D02YN77, Ireland

† Authors contribute equally.

The capacity for the osteogenic differentiation of mesenchymal stem cells (MSCs) by CS/Coll hydrogels is crucial for bone regeneration. The bioactivity of hydrogels relies on the interactions between their molecules and osteoblastic progenitors.[17] Incorporating protein growth factors can improve the therapeutic efficacy,[18,19] but these hydrogels have significant drawbacks, like instability, short life, immunogenicity, and high cost.[20] For example, Jung et al.[21] studied the effect of the bone morphogenetic protein-2 (BMP-2) on the osteogenic differentiation of stem cells and found that the short half-life of BMP-2 protein resulted in a rapid loss of osteogenic differentiation activity. On the other hand, the incorporation of synthetic nanoparticles in to the natural polymer matrix can improve the structural properties of the matrix and mechanism of bone formation and osteoblastic differentiation.[22] For instance, Garcia-Astrain et al.[23] prepared a gelatin hydrogel using silver nanoparticles (AgNPs) as a crosslinking agent and reported that the addition of AgNPs significantly improved the mechanical properties of the hydrogels. Also, Kaur et al.[10] developed injectable CS/Coll hydrogels reinforced with single-wall carbon nanotubes to enhance the mechanical properties of the hydrogels, and reported an increase in cell proliferation and the differentiation of fibroblasts with the addition of nanotubes in the prepared hydrogels.

Selenium nanoparticles (Se-NPs) have emerged as promising materials in the field of bone regeneration due to their antioxidant properties that can help tackle oxidative stress-induced apoptosis in bone regeneration and wound healing.[24,25] Recently, Se-NPs and Se-modified biomaterials were shown to promote osteoporotic and osteonecrosis bone defect repair with higher stability and efficacy.[26–28] Hu et al.[29] developed a hyaluronic acid-based hydrogel loaded with Se-NPs for osteoarthritis treatment via the expression of selenoproteins, and found that the hydrogels facilitated cartilage repair through synergetic effects of scavenging reactive oxygen species and depressing apoptosis through the Se-NPs. Se-NPs can enhance bone remodeling by supporting cellular adhesion and proliferation, matrix mineralization, and osteogenic differentiation, though the optimal concentration and self-renewal of MSCs in Se-NPs-functionalized hydrogels remain unknown at present.[25,30,31]

A new strategy is required to accelerate bone regeneration by providing an osteogenic microenvironment using thermogels that can enhance MSCs differentiation. Previous studies have explored thermoresponsive injectable hydrogels with elemental Se and Se-NPs for stem cell culture, osteoporosis, and bone regeneration under oxidative stress conditions.[28,32] However, to the best of our knowledge, the osteogenic differentiation of MSCs from ovariectomized (OVX) and Sham rats without oxidative stress has not yet been reported. Further, despite numerous publications on CS/Coll hydrogels, either alone[33,34] or with Se and Se-NPs,[25,28,35] there is no reported work on injectable, biodegradable, bioactive hydrogel combining CS, Coll, and varying concentrations of Se-NPs.

This work represents a significant advancement in the field of biomaterials and regenerative medicine. In this study, novel hydrogels functionalized with selenium nanoparticles (Se-NPs) at different concentrations (0, 1.26, and 2.53 mM) were prepared and specifically aimed at promoting the osteoblastic differentiation of MSCs. By integrating the advantageous properties of CS/Coll with Se-NPs, these hydrogels could effectively address the structural and stability challenges commonly associated with natural polymer-based hydrogels. The resulting hydrogels were not only thermoresponsive and biocompatible but presented a promising innovative option as an injectable bone void filler, facilitating minimal invasive regenerative application in diseased bone and advancing the field toward more efficient and patient-friendly therapeutic options.

Dr Subhadeep Roy currently holds the position of Assistant Professor in the Department of Pharmacology and Toxicology at the National Institute of Pharmaceutical Research in Kolkata, India. He received his PhD from Babasaheb Bhimrao Ambedkar University, Lucknow, where he investigated the role of polyunsaturated fatty acids in estrogen receptor-positive breast cancer. He has also worked as a visiting senior research fellow at the ID3S laboratory, Translational Health Science and Technology Institute, Faridabad, in targeted drug delivery and compartment trafficking in human pulmonary macrophages. He has completed his postdoctoral program at IIT, Delhi, and Pennstate College of Medicine, USA. He has authored numerous works in internationally recognized journals that undergo rigorous peer review. Additionally, Dr Roy has received several notable honours and recognitions. Dr Roy's research area focuses on 3D microphysiological disease models, tissue engineering, additive manufacturing and bioinspired/biomimetic cutting-edge translational pharmaceutical research.

Subhadeep Roy

2. Experimental

2.1. Synthesis of selenium nanoparticles (Se-NPs)

The Se-NPs were prepared in the laboratory via a reduction method using sodium selenite (Na_2SeO_3) as a precursor.[36] Ascorbic acid of biological grade was used as a reducing agent and polysorbate 80 as a stabilizer in the reduction chemical reaction. In a typical experiment, 1.26 and 2.53 mM solutions of Na_2SeO_3 were prepared in 450 ml of deionized water to prepare two concentrations of Se-NPs (0.575 and 1.154 mM), respectively. Ascorbic acid (56.7 mM) was added dropwise (2 ml/3 minute) to the sodium selenite solution with vigorous stirring. Next, 10 μL of polysorbate 80 was added after each 2 ml of ascorbic acid. The formation of the Se-NPs was confirmed by a color change from clear white to intense orange. Afterwards, the solution was centrifuged at ∼13 000 rpm to collect the Se-NPs in a pellet form, and this was stored at 4 °C until further use. All the

This journal is © The Royal Society of Chemistry 2024

J. Mater. Chem. B, 2024, **12**, 9268–9282 | **9269**

reagents used were of analytical grade (AR) and used without any further purification.

2.2. Synthesis of the Se-NPs-loaded thermoresponsive hydrogels

CS (2 wt/v%, Sigma Aldrich) and Coll (4 mg ml^{-1}, Integra life science) were dissolved in 0.02 M and 0.1 M acetic acid (Sigma Aldrich) to obtain the desired solution concentrations and labeled as solution I and solution II, respectively. Solution I was mixed with solution II in a volumetric ratio of 98:02 and labeled as solution III. Two different concentrations of Se-NPs pellets (prepared in Section 2.1) were added into solution III individually followed by 24 h stirring to prepare the Se-NPs-functionalized hydrogel solution. Precooled 58 wt% β-glycerophosphate (β-GP, Sigma Aldrich) sodium salt was next added as a crosslinking agent while maintaining the pH at 7.4 for the hydrogel solution. Pure CS and Coll hydrogel solutions added in the same ratio as for solution III, i.e., 98:02, served as the control hydrogel prepared by following the same procedure but without the addition of the Se-NPs. All the syntheses were carried out on ice (∼4 °C) to maintain a liquid state of the prepared hydrogel solutions. The chemical compositions of the prepared hydrogels are given in Table 1, while Fig. 1 presents the steps followed to prepare the Se-NPs and hydrogels. Gelation of the prepared hydrogels was initiated by incubating the solutions at 37 °C for ∼5 min. Gel formation and the time taken were assessed by the mobility of the solution after inverting the tubes.

3. Characterization

3.1. Dynamic light scattering

The particle-size of the prepared Se-NPs was measured using a Zetasizer Nano-ZS system (Malvern Instruments). Se-NPs pellets prepared in Section 2.1 were homogeneously dispersed in phosphate buffered solution (PBS) at pH ∼ 7.4 at room temperature. The obtained homogeneous suspension was then used for recording the particle-size values.

3.2. Transmission electron microscopy

Transmission electron microscopy (TEM) analysis was undertaken to investigate the morphological properties of the prepared Se-NPs. A suspension of the Se-NPs was prepared in distilled water. A drop of homogeneous suspension was dropped onto a copper grid and the grid was dried at room temperature for 24 h followed by analysis using a Hitachi HT7800 transmission electron microscope at room temperature. Image J software was used to analyze the obtained micrographs.

3.3. Rheological analysis – sol to gel transition and injectability

The liquid to gelation transition of the prepared hydrogels with increasing concentration of Se-NPs from 0 to 2.53 mM was assessed using an HR-1 Discovery Hybrid Rheometer (TA instruments) as a function of temperature. Parallel plate geometry (20 mm) was used during the experiment to determine the gelation temperatures of the samples. An oscillation assay was carried out by applying a heating ramp from 4 °C to 45 °C at a heating rate of 1 °C min^{-1}. To stimulate body conditions and to obtain undisturbed gel formation, a 1 Hz frequency and a small strain of 0.01% were applied during the experiment.[37] The storage modulus (G') and loss modulus (G'') were obtained during the heating ramp as a function of temperature. To determine the injectability, the hydrogels were submitted to a flow sweep assay at 37 °C. The change in viscosity was noted as a function of stress. For the gelation time, strain sweep and time sweep tests were performed. For the strain sweep test, the hydrogels were submitted to an oscillation assay at 37 °C with varying the strain from 0.01% to 100%. The obtained results were plotted on a graph using GraphPad Prism software.

3.4. Attenuated total reflectance – Fourier-transform infrared (ATR-FTIR) spectroscopy

ATR-FTIR spectra of the Se-NPs and prepared hydrogels were recorded at room temperature on a NiCOLET iS10 Smart iTX FTIR instrument (Thermo Scientific) in the wavenumber range of 400–4000 cm^{-1}. Origin 8.5 software was used for correcting the baseline and drawing the graphs of each spectrum.

3.5. Scanning electron microscopy (SEM)

SEM analysis was carried out on a JEOL SRX-8 machine to image the structural architecture of the prepared hydrogels. A gold coating was used to make the hydrogels conductive to evaluate their surface morphology.

3.6. *In vitro* cell cytotoxicity and proliferation assay

Rat mesenchymal stem cells (rMSCs) and ovariectomized rMSCs (rMSCs^{OVX}) were isolated from the bone marrow of 6–8-weeks-old male Sprague–Dawley rats and ovariectomized 6–8-weeks-old female Sprague–Dawley rats as previously described.[38,39] rMSCs and rMSCs^{OVX} were maintained in DMEM high glucose supplemented with 20% fetal bovine serum (FBS), 1% antibiotic, 1% glutamax, 1% amino acids, and 0.2% Primocin, and maintained at 37 °C with 5% CO$_2$. At 80% confluence, first, the *in vitro* cytotoxicity of Se-NPs was tested in 2D. In a typical experimental setup, Se-NPs were added

Table 1 Chemical compositions of the prepared hydrogels

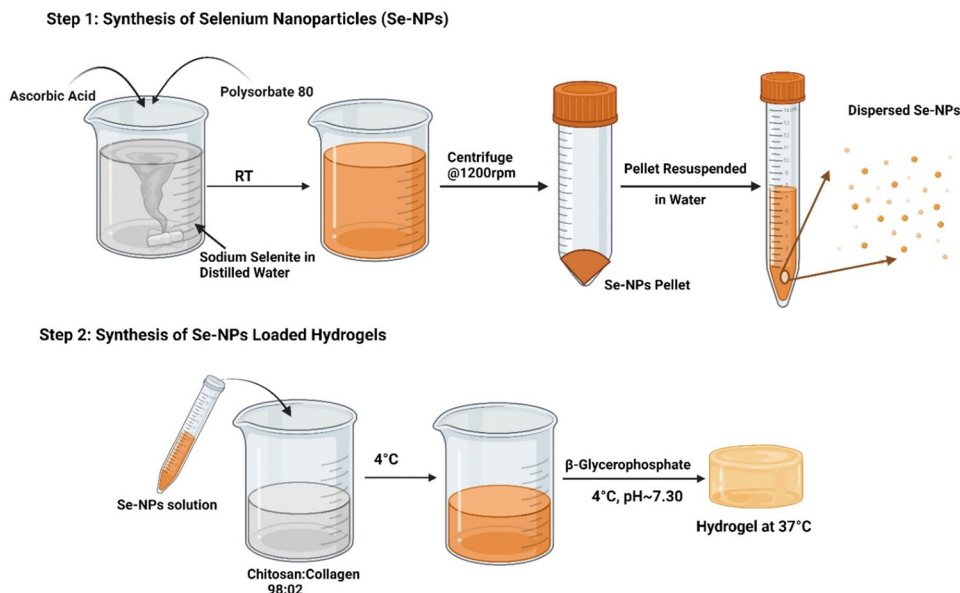| Sample code	Sample description	Chitosan (w/v)%	Collagen (w/v)%	Sodium selenite (mM)	Se-NPs (mM)	Se-NPs (w/v)%
S0	Coll-CS	2.0	0.5	—	—	—
S1	Coll-CS/low Se	2.0	0.5	1.26	0.575	0.045
S2	Coll-CS/high Se	2.0	0.5	2.53	1.154	0.091

Fig. 1 Schematic diagram showing the steps followed for the synthesis of the Se-NPs and hydrogels.

into a DMEM high glucose cell growth medium (10 μL of Se-NPs per 50 ml of growth medium). Briefly, 1×10^5 cells (rMSCs and rMSCs^{OVX}) were seeded in a 12-well adherent tissue culture plate with growth medium supplemented with sterilized Se-NPs. Cells with the growth medium only were used as the positive control. At days 1, 2, and 3 post-seeding, the cell metabolic activity was assessed using an Alamar blue assay (Alamar blue assay kit, Invitrogen) according to the manufacturer's instructions. In brief, the growth medium was removed from the wells followed by washing with PBS. Next, 10% Alamar blue solution ~ 2 ml was added into the washed wells and incubated at 37 °C for $\sim 1–2$ h protected from direct light followed by the transfer of 100 μL of each sample medium to a 96-well black flat bottom plate in triplicate. The fluorescence was recorded at an excitation of 545 and with emission at 590 nm using a plate reader. For the 3D culture, Se-NPs-functionalized hydrogels were used. Here, 3×10^5 cells were seeded on both sides of the hydrogels in a 24-well non-adherent tissue culture plate to avoid the attachment of cells to the well plate. Hydrogels without Se-NPs were used as a positive control. The *in vitro* cytotoxicity was assayed using the Alamar blue assay following the same procedure as explained above. The experiment was conducted in triplicate.

Cell proliferation *via* DNA quantitation was assessed using a Quant-iT™ Pico Green® assay kit (Invitrogen). DNA quantification was assessed over a 1, 3, and 7 day culture period for the 2D and 3D cultures to indirectly measure the proliferation of rMSCs and rMSCs^{OVX} according to the manufacturer's instructions. At 1, 3, and 7 days post-seeding, the medium was removed, and the wells in the 2D and 3D cultures were washed with PBS followed by the addition of pico green lysis buffer and then stored at -80 °C. Three freeze–thaw cycles were performed before running the assay. Fluorescence was recorded at an excitation of 485 and emission at 538 nm on a fluorescent plate reader. Hydrogels without Se-NPs were used

as a positive control. The experiment was conducted in triplicate.

3.7. *In vitro* osteogenic potential

To investigate the therapeutic potential of the prepared Se-NPs-functionalized hydrogels in osteogenic differentiation and the bone-forming activity of rMSCs (rMSCs and rMSCs^{OVX}), the hydrogels were seeded with 3×10^5 cells and cultured in a medium containing osteogenic growth factors, such as 1% β-GP, 0.5% ascorbic acid, and 50 μL dexamethasone for up to 28 days. At 7, 14, 21, and 28 days post-seeding, the hydrogels (in triplicate) were collected for extracellular matrix mineralization and qRT-PCR gene expression analysis. After each time point, to determine the production of extracellular matrix mineralization, the hydrogels were washed with PBS and lysed with 0.5 M hydrochloric acid and the extracellular matrix mineralization was measured using a Syntec calcium (cpc) liquicolor test kit according to the manufacturer's instruction. For alizarin red staining (ARS) on day 28, the hydrogels were collected and fixed. The mineralized matrix formation was determined by ARS staining of cultured rMSCs and rMSCs^{OVX} to detect the deposited calcium.[40] Briefly, the hydrogels were washed with PBS and then fixed with 10% formalin. The fixed hydrogels were sectioned and stained with 2% ARS solution for 15 min, then washed twice with deionized water, and observed under a Motic AE31E microscope equipped with a LEICA DFC420 camera. For qRT-PCR gene expression, total RNA was isolated using an RNeasykit according to the manufacturer's instructions. The target mRNAs analyzed were runt-related transcription factor 2 (RUNX2), alkaline phosphatase (ALP), bone morphogenetic protein 2 (BMP2), and osteocalcin (OCN), with 18s used as a housekeeping gene. A list of the primers that were used for amplification of these genes is

Table 2 List of gene transcripts analyzed by qRT-PCR

Target proteins	Abbreviation	Target gene reference	Catalogue reference
18S	18S	Rn_Rn18s_1_SG	QT02589300
RUNX family transcription factor 2	RUNX2	Rn_Runx2_1_SG	QT01620647
Alkaline phosphatase	ALP	Rn_Alppl2_1_SG	QT00458892
Osteocalcin	OCN	Rn_bglap_1_SG	QT00371231

provided in Table 2. The experiment was conducted in triplicate.

3.8. *In vitro* biocompatibility with fibroblast co-culture

The *in vitro* biocompatibility of the prepared functionalized hydrogels was measured in a co-culture of mouse embryonic fibroblast (MEF)/McCOY (adult healthy human fibroblast)/Rat bone marrow-derived stem cells (BMSCs) (National Center for Cell Science, Pune, India) in 24 mm (5 μm) 6-well inserts (Merck). Briefly, following ISO standard 10993/10933-5, the functionalized hydrogels (∼4 mg) were incubated with MEF/McCOY/Rat BMSC cells for 48 h at 37 °C with 5% CO_2. A cocktail of the cells MEF/McCOY/Rat BMSC was added to the basal chamber and the hydrogels were placed in the apical chamber of the trans-well to study the hydrogel/cell interactions. After 48 h, a live/dead assay was performed (live/dead viability kit, Invitrogen) to determine the effect of the hydrogels on the biocompatibility of the cells based on the plasma membrane integrity and esterase activity according to the manufacturer's instructions, followed by Hoechst 33258 staining and imaging using a Leica DMi8 STELLARIS 5 confocal microscope.

3.9. Cell surface marker analysis

The prepared hydrogels were cultured with BMSCs in a trans-well for a period of 48 h followed by fixation with the Image It Fixation kit (Invitrogen) for 15 min away from light and overnight incubation for blocking using Straight Block BSA (Invitrogen). CD 105 (1 : 500, Invitrogen), CD90 (1 : 250, Invitrogen), CD73 (1 : 100, Invitrogen), CD45 (1 : 500, Invitrogen), and CD34 (1 : 500, Invitrogen) were used as primary antibodies and Alexa Flour 588 as the secondary antibody. The hydrogels were coated with gold anti-fade reagents (Invitrogen) prior to processing by confocal imaging (Leica DMi8 STELLARIS 5).

3.10. Statistical analysis

The data are presented as the mean ± standard error of the three experimental values. Statistical analysis of the data was performed with one-way analysis of variance (ANOVA), and p-values less than 0.001 and 0.01 were considered significant.

4. Results and discussion

4.1. Microstructure analysis

4.1.1. Synthesis of selenium nanoparticles. Se-NPs were prepared by a wet chemical reduction method, which is a very simple and inexpensive method. In a typical reaction, sodium selenite in the aqueous medium formed selenium oxyanions that react with ascorbic acid and are reduced to elemental selenium (Se^0), which is stabilized by polysorbate 80. TEM confirmed the monodispersed and homogeneous spherical structure of the as-prepared Se-NPs as shown in Fig. 2(a) and (b). This conversion of sodium selenite into Se-NPs was also confirmed by a color change from transparent to orange, as shown in Fig. 2(c). The synthesized particles had an average size of 106.2 nm with a polydispersity index (PDI) of 0.014, as confirmed by DLS analysis (Fig. 2(d)).

4.1.2. Fabrication of Se-NPs-functionalized thermoresponsive hydrogels. Thermoresponsive hydrogels are *in situ* gelling systems made of a hydrophilic homopolymer or block copolymers, which behave as a liquid at room temperature but turn into a gel at physiological temperature (37 °C). In this work, thermoresponsive hydrogels of CS/Coll, with a volumetric ratio of 98/02 and containing different concentrations of Se-NPs (0, 1.26, and 2.53 mM) were formulated for transition to a stable gel state at 37 °C with the addition of β-GP. β-GP has previously been reported to confer thermoresponsivity to Coll- and CS/Coll-based hydrogels.[41] The prepared hydrogels remained liquid at room temperature but became solid gels after incubation at 37 °C for 5 min. This phase transition was initially assessed visually by inverting the tubes containing the prepared hydrogels, as shown in the inset of Fig. 3(a)–(c). The S0 hydrogel was white in color, whereas the Se-NPs-containing hydrogels became an intense orange color due to dispersion of the orange-colored Se-NPs solution in the polymeric matrix. Upon inverting the tube, the hydrogel formulations remained fixed to the bottom of the tubes, indicating that the hydrogels had gelled at 37 °C and that the inclusion of Se-NPs into the CS/Coll polymeric matrix did not interfere with the thermoresponsivity of the hydrogels at 37 °C, as shown in Fig. 3(a)–(c). The pH of the polymeric solution before and after gelation was in the range of 6.95 ± 0.02 to 7.38 ± 0.02, as recorded using a CyberScan 510 pH meter. These values of pH ensured that (i) no significant change in the pH value occurred after conversion of the liquid to solid gel at 37 °C, and also (ii) that the addition of Se-NPs did not lead to any undesired pH-sensitive chemical reactions occurring, which could have otherwise changed the structure or pH of the polymeric matrix during the gelation process. In the typical gelation mechanism as reported earlier,[10] as the temperature increases, it leads to an increased ionic strength *via* the ionization of β-GP, causing a change in the pH to provide a favorable environment in which the 3D gel network can form while enhancing the polymer–polymer interactions through a hydrophobic effect. Therefore, hydrophobic interactions are a key factor to form gels consisting of CS/Coll/Se-NPs and β-GP at 37 °C.

9272 | *J. Mater. Chem. B*, 2024, **12**, 9268–9282

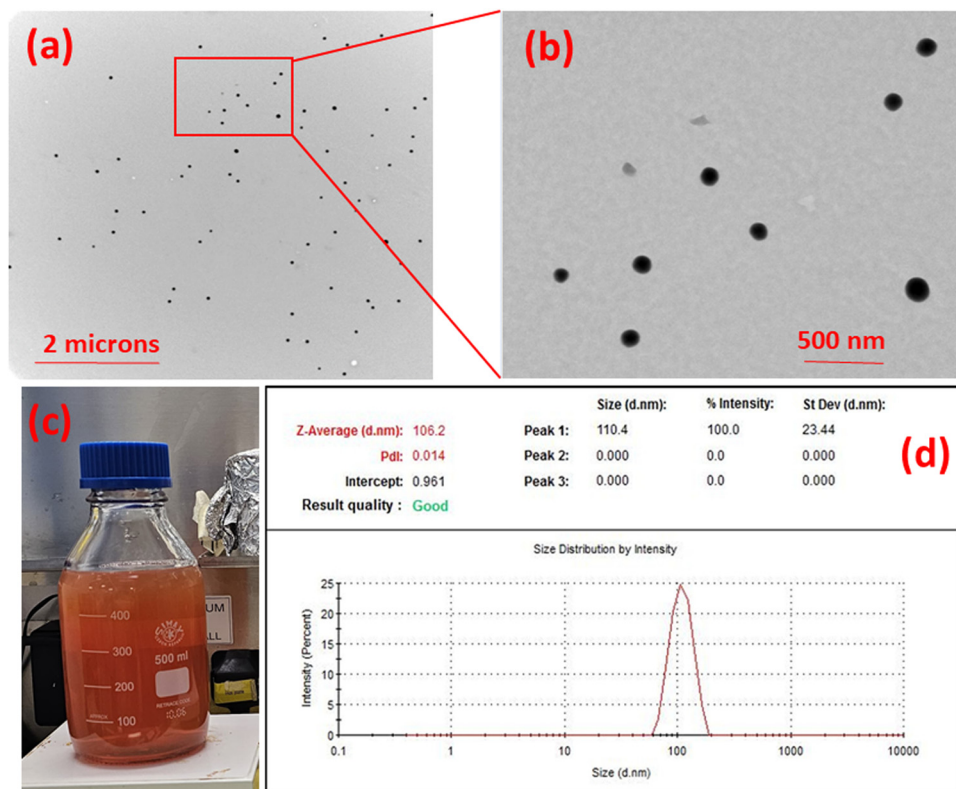This journal is © The Royal Society of Chemistry 2024

Fig. 2 TEM micrograph of the prepared Se-NPs at (a) 2 microns and (b) 500 nm magnification. (c) Intense orange-colored Se-NPs solution and (d) particle-size analysis of the prepared Se-NPs measured by dynamic light scattering.

Rheological analysis. Rheology analysis was used to investigate the gelation and elastic behavior of the prepared Se-NPs-functionalized hydrogels. The rheology was assessed by measuring the storage modulus (G') and loss modulus (G'') as a
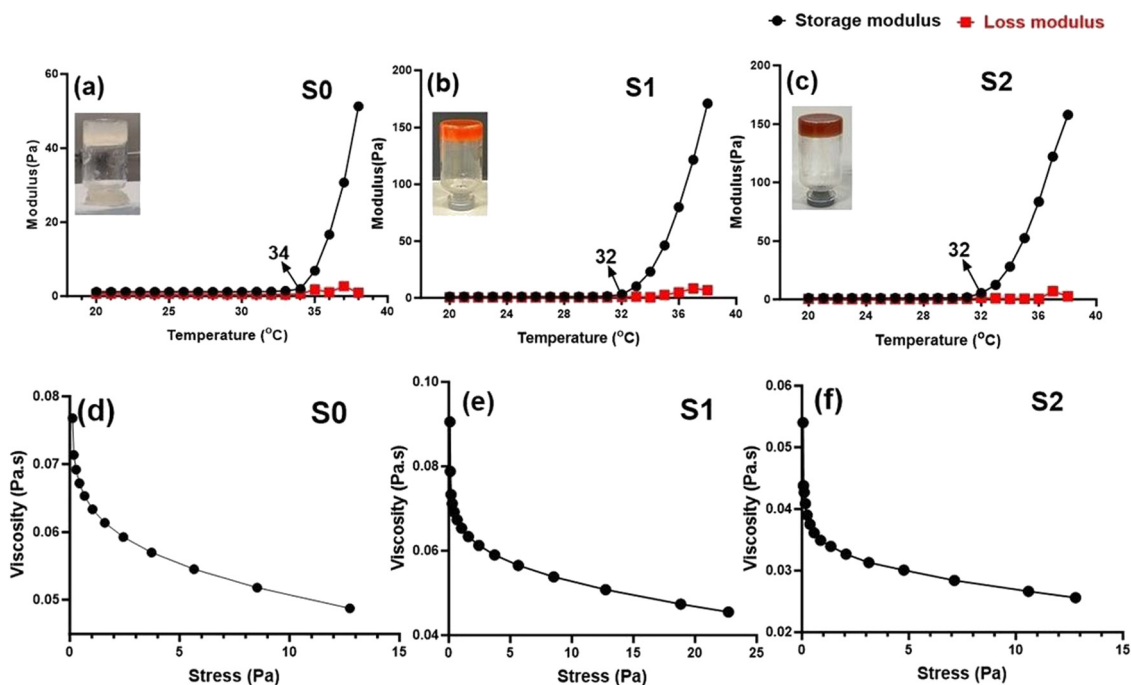

Fig. 3 (a)–(c) Storage modulus and loss modulus of the prepared hydrogel solutions as a function of temperature. The intersection points are indicative of the gel formation temperature. (d)–(f) Changes in the viscosity of the hydrogel solution as a function of stress.

This journal is © The Royal Society of Chemistry 2024

J. Mater. Chem. B, 2024, **12**, 9268–9282 | **9273**

function of temperature from 20 °C to 38 °C (Fig. 3(a)–(c)). The variation of both the G' and G'' curves did not change with the addition of Se-NPs, and mainly the curves contained two regions. The growth rate of G' was much higher than that of G'', signifying that the evolution of the gel structure primarily contributed to the increase in the elasticity of the prepared hydrogel systems.[42] The gelation temperature of the prepared hydrogels is defined as the temperature at the crossover of the G' and G''. Fig. 3(a)–(c) shows the gelation temperature of the prepared hydrogels along with the values of G' and G'' in the temperature range of 20–38 °C. The functionalization of the prepared hydrogels with Se-NPs resulted in an increase in G', which implied an increase in the elasticity of the hydrogel. In the second and last region, the increasing temperature led to an increase in ionic strength *via* the ionization of β-GP, causing a change in the pH to provide a favorable environment for the elastic 3D gel network to form. This driving force behind the process was the reduction in CS/Coll solubility, and the increased hydrophobic interactions.[10]

The injectability (the ability to be extruded) of the formulated elastic hydrogels was also evaluated from rheological analysis by a flow sweep test at room temperature. In Fig. 3(d)–(f), it can be seen that all the prepared hydrogels exhibited a rapid decrease in viscosity upon the application of shear stress. The thermoresponsive and injectable properties of the prepared hydrogels offer a promising potential to be used in a minimally invasive approach for bone tissue engineering applications.

4.1.3. ATR-FTIR analysis. In order to illustrate interactions between the components in the hydrogels, ATR-FTIR spectra were recorded. Fig. 4 shows the ATR-FTIR spectra of the Se-NPs and Se-NPs-functionalized freeze-dried hydrogels. The observed vibration bands together with their corresponding structural units are provided in Table 3. The Se-NPs were characterized by ATR-FTIR to confirm the presence of functional groups responsible for the synthesis and stability of the Se-NPs. The Se-NPs showed an intense peak at ~3350 cm^{-1} attributed to hydroxyl group stretching of the aromatic ring of ascorbic acid. Other peaks observed were at 1740 cm^{-1} representing stretching of a C=O aldehyde group, 1630 cm^{-1} due to amide and C–H vibrations of a CH$_2$ group, and 1405 cm^{-1} (C–H), 1240 cm^{-1} (secondary OH bending), and 1053 cm^{-1} (C=O) stretching vibrations.[43,44] All the observed peaks and bands in the Se-NPs spectrum confirmed the formation of stable Se-NPs. In the prepared hydrogels, the presence of amide I (stretching vibrations of C=O) bands in the wavenumber range of 1620–1700 cm^{-1} was generally due to CS and Coll, while those at 1510–1580 cm^{-1} for amide II corresponded to N–H bending and C–N stretching vibrations, and those at 1350–1380 cm^{-1} were mainly related to C–N stretching.[45] The FTIR spectrum of the Coll-CS scaffolds with Se-NPs was similar with the bands of Se-NPs, albeit slightly different in intensity due to the interactions between the Se-NPs and CS/Coll polymeric matrix. It could be clearly observed from Fig. 4 that the prepared Se-NPs-functionalized hydrogels showed a broadband signal at ~3200 cm^{-1} corresponding to the stretching of intermolecular bonded OH combined
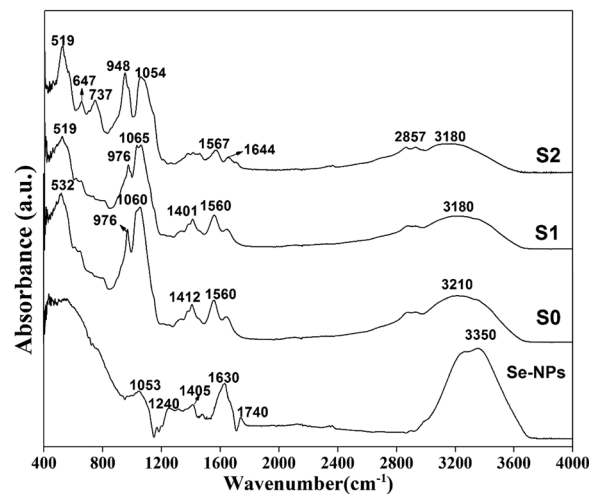

Fig. 4 ATR-FTIR spectra of the prepared Se-NPs and Se-NPs-functionalized freeze-dried hydrogels.

with NH groups.[46] Symmetric stretching vibrations appeared at 2857 cm^{-1} corresponding to aliphatic CH$_2$ groups. However, the peaks at ~1560 and ~1400 cm^{-1} could be attributed to N–H and O–H bending, respectively, while the peaks at ~1740 and ~1050 cm^{-1} corresponded to C–O and COO stretching.[47] A red-shift in the spectrum of the prepared hydrogels could be seen with the addition of Se-NPs (Fig. 4), as reported in Table 3. In addition, a shift at higher wavenumber was observed corresponding to vibrations of the hydroxyl groups of the polymer, indicating their participation in the stabilization of the Se-NPs. Also, the peak at 1630 cm^{-1} in the Se-NPs spectrum was shifted to 1644 cm^{-1}, indicating the formation of Se–O bonds in the Se-NPs-functionalized hydrogels, which also implied the stabilization of the Se-NPs inside the polymeric matrix.[48]
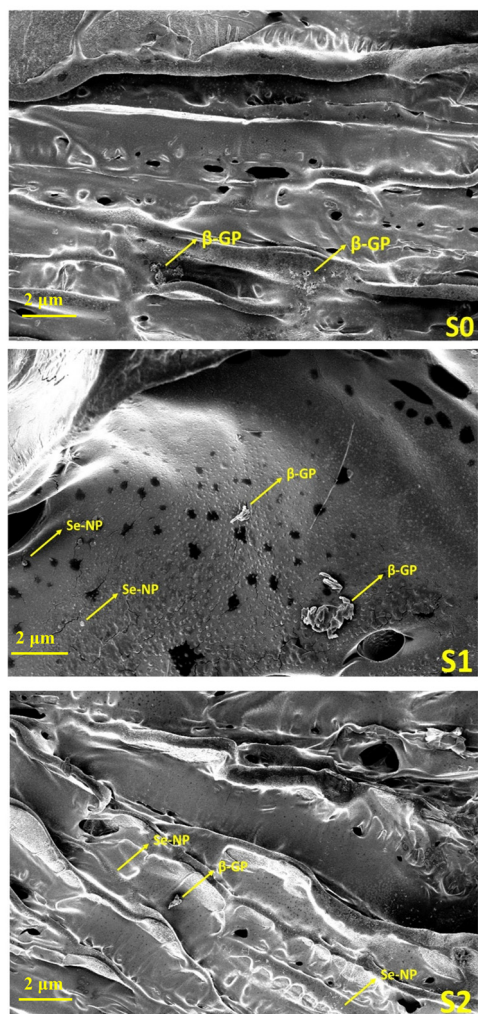
4.1.4. SEM analysis. The highly porous and homogeneous interconnected structure of the prepared freeze-dried hydrogels was analyzed by SEM. Fig. 5 shows representative SEM images of the S0, S1, and S2 hydrogels. The microstructures of the hydrogels showed the presence of precipitations of crystals on the surface of the polymeric matrix due to β-GP, suggestive of the presence of ammonium phosphate or sodium phosphate due to coating the polymer chains with the divalent β-GP. Moreover, the images indicated the porous structure. The SEM showed that the functionalization of the prepared hydrogels with Se-NPs improved the overall morphology (pore structure and interconnectivity) with the presence of bright Se-NPs on the surface. The interconnectivity and stable internal pore channels provide space for infiltrating cells. The pore size and porosity are advantageous for cell adhesion, ingrowth, and proliferation. Furthermore, the importance of a porous structure has been well established in the literature concerning tissue regeneration.[60,61]

4.2. Biological analysis

4.2.1. *In vitro* biocompatibility and osteogenic potential of rMSCs with Se-NPs and hydrogels. For bone tissue engineering with the combination of hydrogels with stem cells, excellent cytocompatibility is one of the most important prerequisites for

9274 | *J. Mater. Chem. B*, 2024, **12**, 9268–9282

This journal is © The Royal Society of Chemistry 2024

Table 3   Observed vibrations in the ATR-FTIR spectra as a function of the wavenumber (cm^{-1})

Structural units	Se-NPs position	S0 position	S1 position	S2 position	Ref.
Stretching of C–O–C between the rings and C–H out of plane vibrations and bending of PO$_4$ group	—	532	519	519	49–51
Stretching of C–O–C between the rings and C–H out of plane vibrations	—	—	—	647	52
Symmetrical stretching and bending of PO$_4^{3-}$ bond and GP aliphatic P–O–C stretching	—	—	—	737	51, 53 and 54
C=O stretching vibrations, aliphatic P–O–C stretching	—	976	976	948	33, 45, 51 and 52
C=O stretching vibrations	1053	1060	1065	1054	43–45
Secondary OH bending	1240	—	—	—	43 and 44
Bending vibrations of CH$_2$	1405	1412	1401	—	43, 55 and 56
Amide II, N–H bending and C–N stretching vibrations of CS and Coll	—	1560	1560	1567	45, 51 and 56
Amide I, stretching vibrations of C=O collagen, overlapping stretching vibrations of amide I and molecular water	1630	—	—	1644	10, 46 and 57
Stretching of C=O aldehyde group	1740	—	—	—	43 and 44
C–H stretching vibrations		2857	2857	2857	55, 56 and 58
OH vibrations of adsorbed water, stretching vibrations of N–H and C–H groups overlapped with broad O–H vibrations, O–H stretching of the aromatic ring of ascorbic acid	3350	3210	3180	3180	33, 43, 44, 51 and 59

Fig. 5   Representative SEM images of Se-NPs-functionalized freeze-dried hydrogels at 50 μm magnification. Arrow indicates the presence of bright Se-NPs and β-GP crystals on the surface of the hydrogels.

scaffold materials in order to support cell attachment. Fig. 6(a) shows the cell viability of rMSCs in 2D and on hydrogels using the Alamar blue assay. Alamar blue is based on the reduction of resazurin to fluorescent resorufin after intracellular intake, which produces bright red fluorescent, which is used to quantify cell viability (%). The results showed negligible cytotoxicity in 2D and across the formulated hydrogel range with lower and higher concentrations of Se-NPs. Recently, Tian et al.[62] developed injectable thermosensitive Se-containing hydrogels to carry MSCs for the treatment of limb ischemia, and reported that the prepared hydrogels exhibited favorable biocompatibility, biodegradability, and antioxidant properties at a 2 μM concentration of Se. Above 2 μM, they observed an increase in cytotoxicity, but in our prepared hydrogels with Se-NPs at 2.53 mM of concentration, we found negligible toxicity due to the stable polymeric matrix. Next the pico green assay was carried out to quantify the proliferation of rMSCs in 2D (Fig. 6(b)) and on the hydrogels (Fig. 7(a)). After culturing for 1 day, similar levels of proliferation were observed between S0 and S1. Interestingly, the cell proliferation exhibited an increasing trend in a time-dependent manner, and the DNA content at day 7 was three times as many as that at day 1 in 2D and on the hydrogels. The DNA content in the 3D hydrogels increased significantly due to the stable polymeric matrix and local delivery of Se-NPs, which minimize toxicity. Therefore, cells cultured on the hydrogels showed a better proliferation than those on the 2D platform (p < 0.001). Coll and CS having high biocompatibility and degradability play an important role in cell growth, differentiation, and migration, as reported by Liu and Sun[63] and Kaur et al.[10]

Nanorough Se was reported to promote healthy osteoblast adhesion on titanium disks by Holinka et al.[64] Therefore, the excellent cytocompatibility could be attributed to the chemical components and porous structure of the hydrogels, which provide the suitable environment to support cell adhesion, spreading, and proliferation.[65] Nonetheless, the results indicate that the formulated hydrogels were cell-adhesive and provide a

This journal is © The Royal Society of Chemistry 2024

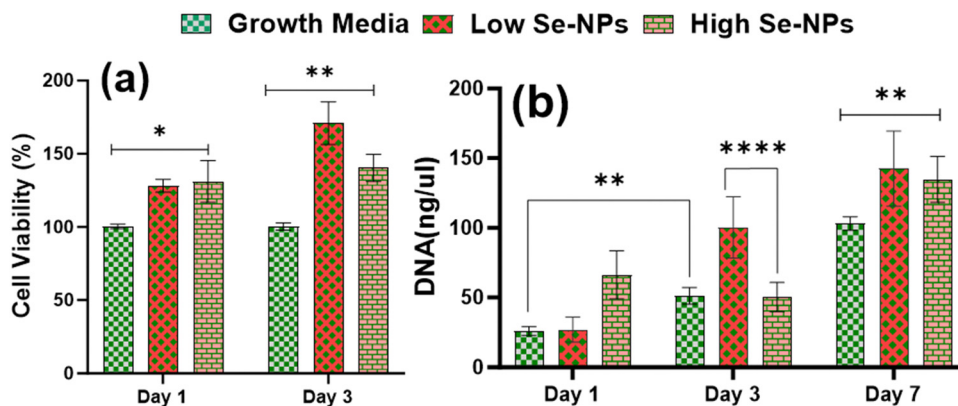*J. Mater. Chem. B*, 2024, **12**, 9268–9282 | **9275**

Fig. 6 (a) Alamar blue activity of the prepared Se-NPs with rMSCs in 2D. (b) DNA quantification of rMSCs in 2D with Se-NPs. Error bars indicate the standard deviation observed for three experimental measurements (*$p < 0.01$, **$p < 0.005$, ***$p < 0.001$).

favorable microenvironment for cell proliferation and survival. Another contributing factor may be the highly interconnected pore structure, which facilitates not only infiltrating cells but also oxygen and nutrients diffusion, which can contribute positively to the health of growing cells. Thus, the combined bioactivity, biocompatibility, and microstructure of the formulated hydrogels may be the reason for the improved cell proliferation.

Due to the low bioavailability of inorganic selenium, organic selenium, a type of selenium that is present in nutrition/foods, is generally more bioavailable than inorganic selenium, and so is more easily absorbed and utilized by the body. Due to these properties, nano-selenium is attracting a lot of interested from researchers. Studies have shown that Se-NPs functionalized with ruthenium(II) and citric acid accelerate stem cell differentiation toward osteogenic lineage.[66–68] *In vitro* research has also shown inhibitory effects of selenium on the growth of many cancer cell lines, but not on normal cells, through

regulating reactive oxygen species as an antioxidant.[32,35,69] As reported by Hou *et al.*,[70] the osteogenic potential of Se-NPs is concentration-dependent in 2D, and we therefore investigated whether the inclusion of Se-NPs without any functionalization into CS/Coll hydrogel would enhance the osteogenic differentiation of rMSCs.

Because of their improved cell viability and ability to support cell spreading and proliferation, only Se-NPs-loaded hydrogels were assessed for effects on the osteogenic properties by measuring calcium mineralization and the expression level of osteogenic-related genes. Calcium mineralization was assessed at days 7, 14, 21, and 28 days post-seeding, as shown in Fig. 7(c). The calcium mineralization of rMSCs on the Se-NPs-loaded hydrogels followed a concentration-dependent trend, whereby with increasing the concentration of Se-NPs, mineralization was significantly enhanced compared to the control hydrogel. The calcium mineralization of rMSCs was also
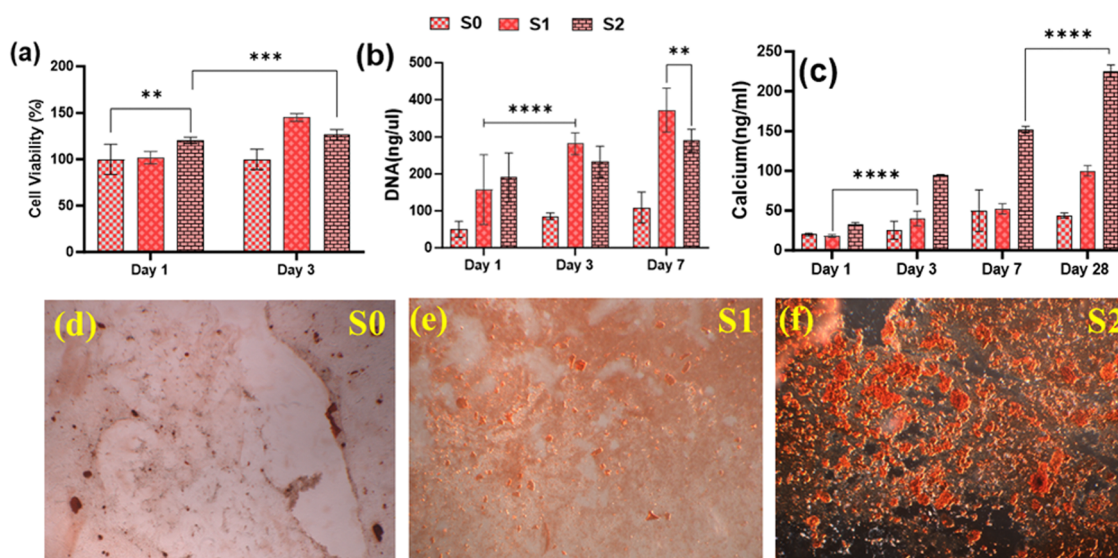

Fig. 7 (a) Alamar blue activity, (b) DNA quantification, (c) calcium mineralization of the prepared hydrogels with rMSCs. (d)–(f) Representative microscopic images (10×) of ARS on the hydrogels after 28 days with rMSCs. Error bars indicate the standard deviation observed for three experimental measurements (*$p < 0.01$, **$p < 0.005$, ***$p < 0.002$, and ****$p < 0.001$).
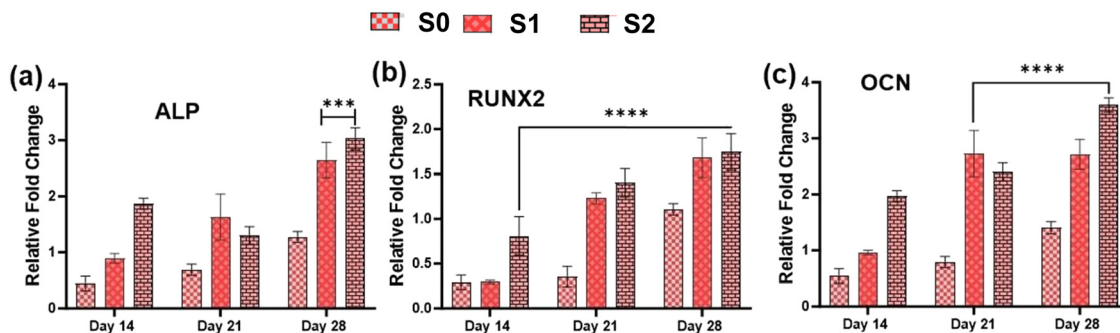
Fig. 8 Evaluation of gene expression by qRT-PCR: (a) ALP, (b) RUNX2, and (c) OCN with rMSCs at days 7, 14, 21, and 28. Error bars indicate the standard deviation observed for three experimental measurements (***$p < 0.002$ and ****$p < 0.001$).

assayed by Alizarin red staining (Fig. 7(d)–(f)). The above results demonstrated that the Se-NPs enhanced the osteogenic potential of the prepared hydrogels. To further investigate the osteogenic effects of the prepared hydrogels, the osteogenic-related gene expression levels were examined. The osteogenic-related gene expression level of the early (RUNX2, ALP) and late (OCN) markers were increased in all the prepared hydrogels from day 14 to 28, as shown in Fig. 8. Notably, the gene expression levels were significantly higher in the Se-NPs-loaded hydrogels (S1 and S2) compared to in S0.

4.2.2. *In vitro* biocompatibility and osteogenic potential of rMSCs^OVX with Se-NPs and hydrogels. To identify whether or not post-menopausal osteoporotic bone marrow-derived cells showed *in vitro* self-renewal and osteogenic potential, we studied the effect of our prepared Se-NPs and hydrogels on OVX bone marrow-derived rMSCs^OVX. Fig. 9(a) and (b) shows the cell cytotoxicity of rMSCs^OVX and DNA quantification in 2D with the Se-NPs-supplemented medium. Fig. 10 shows the cell cytotoxicity (a) and DNA quantification (b) of the Se-NPs-functionalized hydrogels. Our results showed that the Se-NPs and hydrogels were non-toxic to rMSCs^OVX. Interestingly, the cell proliferation and DNA content increased with the addition of Se-NPs in the culture medium as well as in the hydrogels, but only for lower concentrations (1.26 mM). The higher concentration (2.53 mM)

of Se-NPs decreased the DNA content in 2D as well as with the hydrogels, as shown in Fig. 9(b) and 10(b). It was observed from the obtained data that the rMSCs^OVX tended to have slower growth characteristics compared to rMSCs (healthy) as given above. This indicates that the induction of osteoporosis by means of ovariectomy resulted in lower proliferation rates and reduced the capacity of regeneration with the hydrogels. Goregen *et al.*[71] reported similar results upon comparing the growth of sham-derived stem cells and OVX bone-derived stem cells in 2D. They observed that the OVX-derived cells showed slower growth characteristics when investigated by MTT assay. The osteogenic differentiation potential of the prepared Se-NPs and loaded hydrogels with rMSCs^OVX was investigated for up to 28 days.

Similar to the proliferation study, calcium mineralization decreased with increasing the Se-NPs concentration, as shown in Fig. 10(c), and ARS was further done on the hydrogels to confirm the results, as shown in Fig. 10(d)–(f). The differences between the osteogenic potentials of the S0, S1, and S2 hydrogels were highly significant ($p < 0.001$). qRT-PCR analyses showed that the expressions of ALP, RUNX2, and OCN were upregulated in the hydrogels compared to the control, as shown in Fig. 11. It is obvious from the data that the S1 hydrogel had a greater osteogenic differentiation potential with
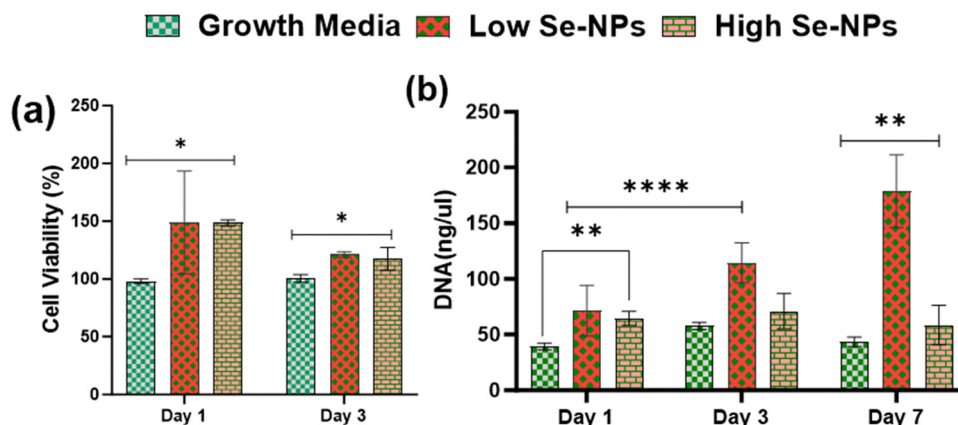

Fig. 9 (a) Alamar blue activity of the prepared Se-NPs with rMSCs^OVX in 2D. (b) DNA quantification of rMSCs in 2D with Se-NPs. Error bars indicate the standard deviation observed for three experimental measurements (*$p < 0.01$, **$p < 0.005$, ****$p < 0.001$).
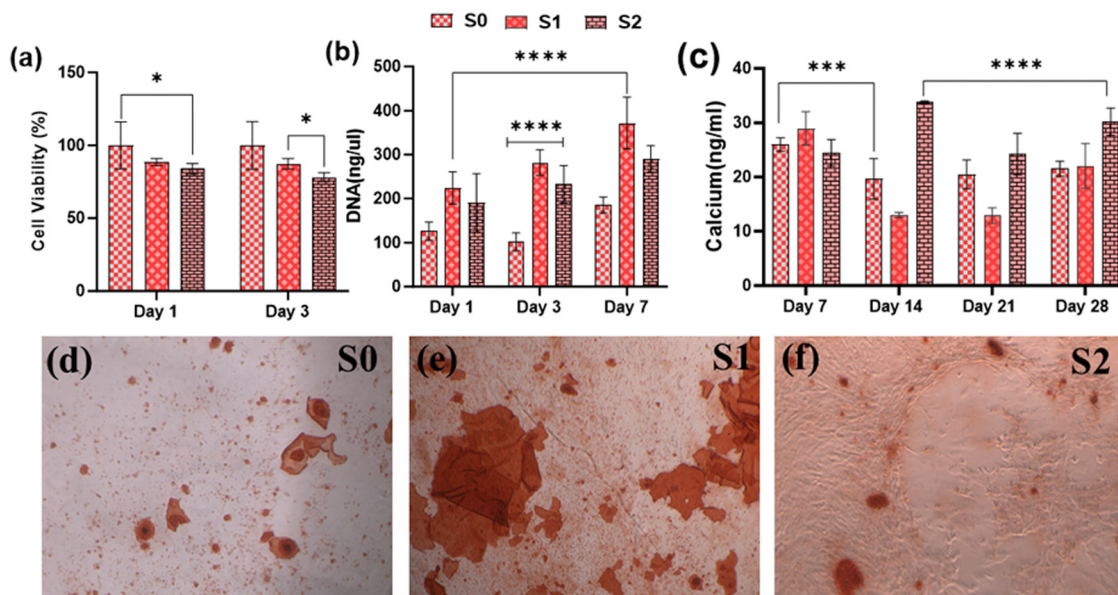
This journal is © The Royal Society of Chemistry 2024

J. Mater. Chem. B, 2024, **12**, 9268–9282 | **9277**

Fig. 10 (a) Alamar blue activity, (b) DNA quantification, (c) calcium mineralization of the prepared hydrogels with rMSCs^{OVX}. (d)–(f) Representative microscopic images (10×) of ARS on the hydrogels after 28 days with rMSCs. Error bars indicate the standard deviation observed for three experimental measurements (*$p < 0.01$, **$p < 0.005$, ***$p < 0.002$, and ****$p < 0.001$).

rMSCs^{OVX}. The lower osteogenic potential of rMSCs^{OVX} compared to the healthy rMSCs was related to the altered mesenchymal stem cells dynamics, as reported by Rodriguez et al.[72,73] The upregulation of gene expressions in S1 indicate that the status of cells with the S1 hydrogel was more toward the osteogenic lineage to compensate for the proceeding bone loss. The present *in vitro* study is preliminary research but further studies are necessary to clarify whether the *in vivo* biocompatibility of rMSCs^{OVX} is also good enough for the regeneration of hard and soft tissues. Our findings though give an indication that rMSCs from post-menopausal osteoporotic hosts could be an option for cellular and genetic therapies for bone regeneration and to develop clinical strategies.

4.2.3. *In vitro* biocompatibility assessment and cell surface marker analysis. The primary objective of this experiment was to examine the biocompatibility with the hydrogel system in a co-culture. All the samples showed a high-intensity green signal from Calcein AM staining, which indicated cellular viability,

and no dead cells were observed in all the prepared hydrogels, as shown in Fig. 12. All the fibroblast exhibited the typical healthy fibroblasts morphology, which consisted of an extracellular projection that was spindle-shaped and elongated, as well as a significant Calcein AM signal. As shown, we can conclude that the hydrogels demonstrated a high level of compatibility with mouse embryonic as well as adult healthy fibroblasts.

After confirming the biocompatibility, we looked into a wide variety of cell surface markers for rat BMSCs. Positive (CD73, CD90, and CD105) as well as negative (CD34 and CD45) markers were expressed by rat BMSCs along with the surface marker (CD73). Upon comparing the results, it was found that CD73+ mouse BMSCs exhibited a greater "stemness" and a greater tendency for osteogenic development *in vitro*.[74] In the process of repairing bone fractures in mice, CD73+ BMSCs showed an increased potential to promote fracture healing.[75,76] We found that the expression of CD73 was noticeably higher in
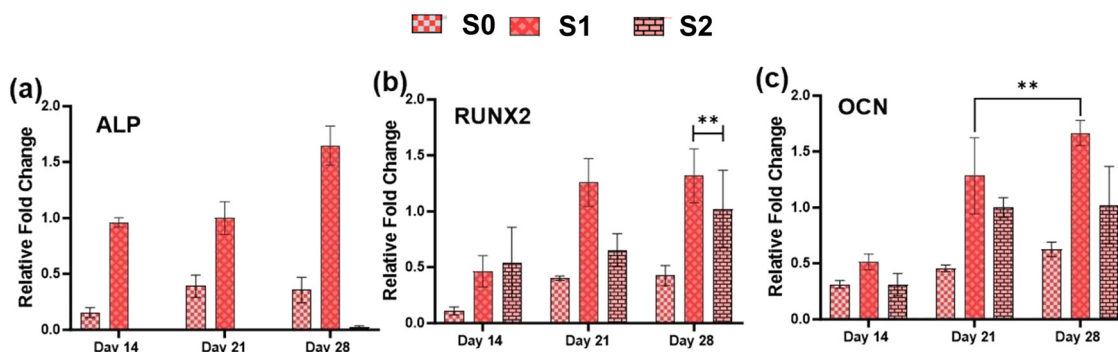

Fig. 11 Evaluation of gene expression by qRT-PCR: (a) ALP, (b) RUNX2, and (c) OCN with rMSCs^{OVX} at days 7, 14, 21, and 28. Error bars indicate the standard deviation observed for three experimental measurements (**$p < 0.005$).

9278 | *J. Mater. Chem. B*, 2024, **12**, 9268–9282
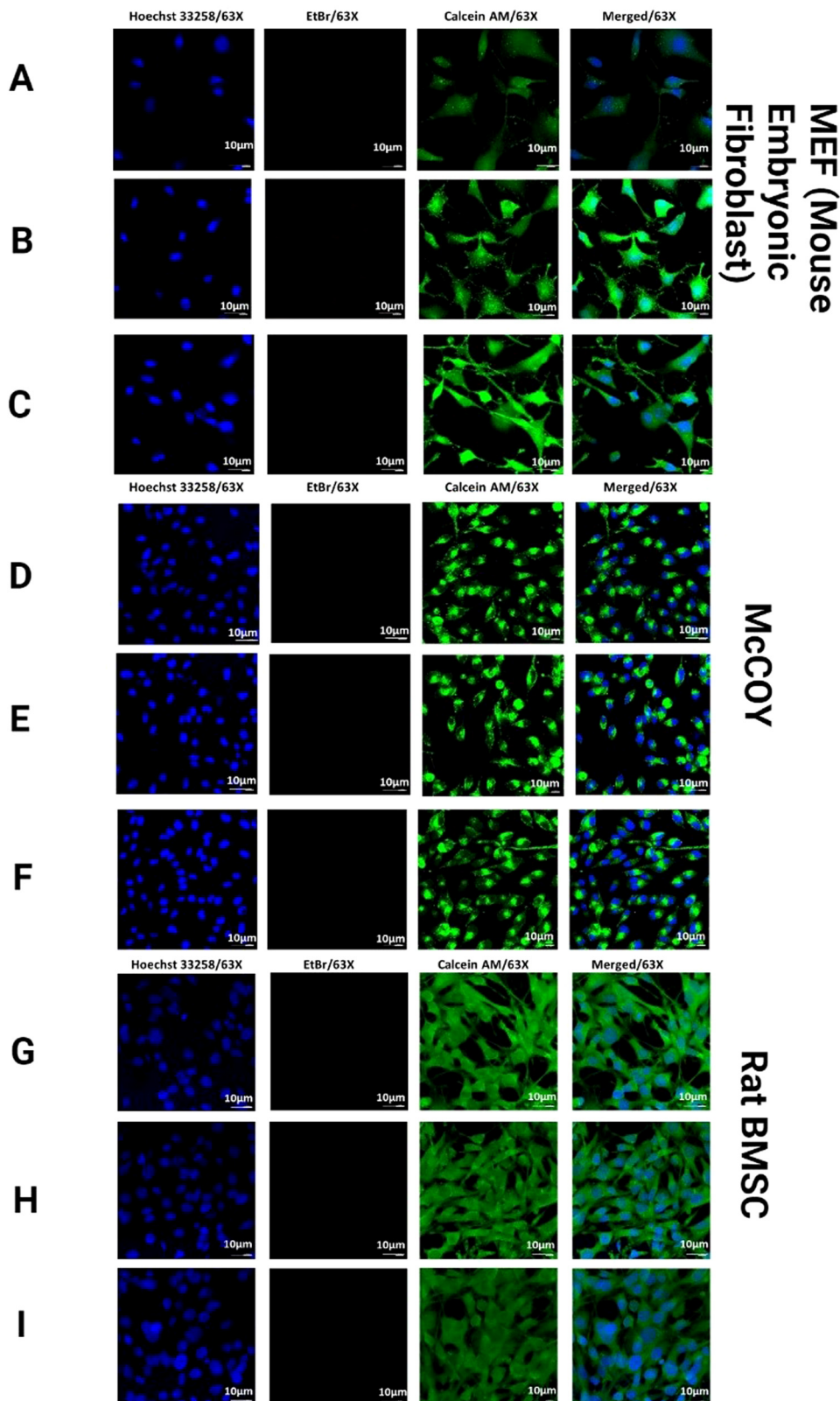
This journal is © The Royal Society of Chemistry 2024

Fig. 12 Three distinct cell types (MEF, McCOY, and Rat BMSC) were used for biocompatibility testing. (A, D and G) represent S0. (B, E and H) represent S1, and (C, F and I) represent S2 hydrogel results. All the samples were captured at 63× magnification in triplicate.

comparison to with the S0 hydrogel, as shown in Fig. 13, confirming the increase in calcium accumulation and gene

expression profile of RUNX2 in the prepared hydrogels. The anti-inflammatory properties of the hydrogels were shown to
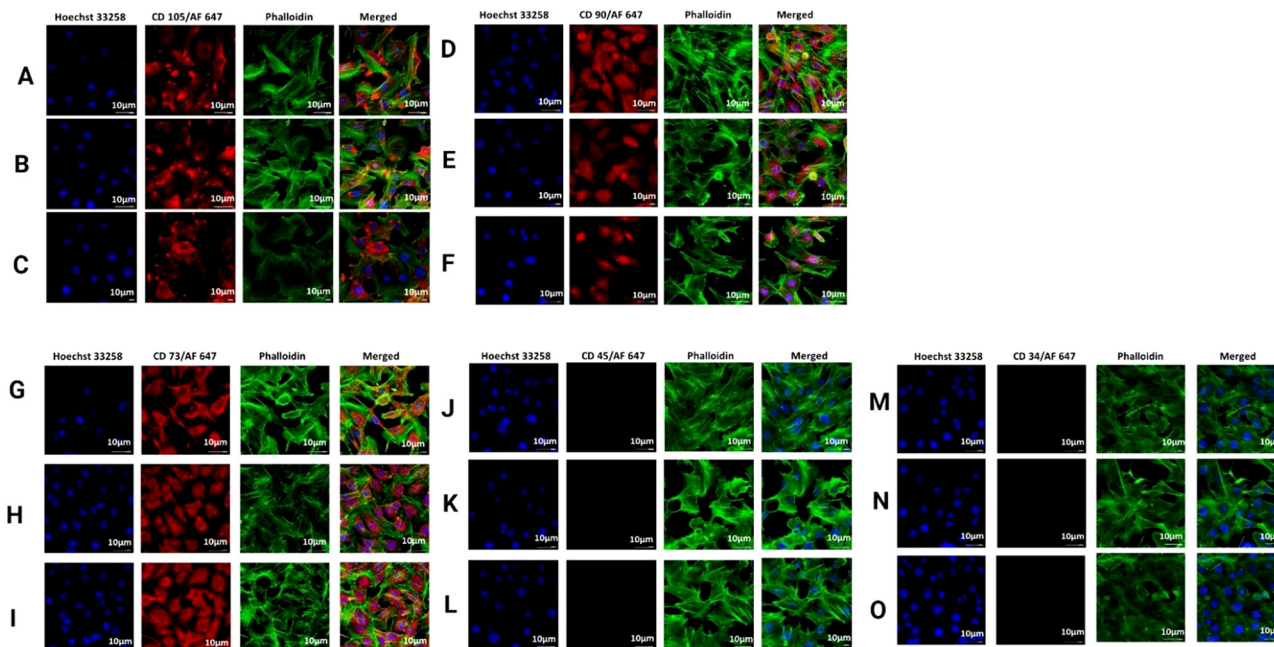
This journal is © The Royal Society of Chemistry 2024

J. Mater. Chem. B, 2024, **12**, 9268–9282 | **9279**

Fig. 13 Immunostaining of CD105, CD90, CD73 (positive), and CD45, CD34 (negative) on rat BMSCs in a *trans*-well co-culture setup with respective to the prepared hydrogels. Images (A, D, G, J and M) represent the S0 hydrogel, images (B, E, H, K and N) represent the S1 hydrogel, and images (C, F, I, L and O) represent the S2 hydrogel results. All the samples were captured at 63× magnification in triplicate.

have a correlation with higher levels of CD73 expression; whereas the expressions of CD105 and CD 90 did not change under any circumstances in all the prepared hydrogels.

Hu *et al.*[70] studied the *in vitro* potential effect of Se-NPs on osteoblast differentiation at different concentrations from 0 to 2048 ppm. They found that Se-NPs at a concentration of 64 ppm or below promoted osteoblast differentiation, whereas at higher concertation they inhibited the expression of RUNX2. Similarly, in the ARS assay, a high concentration of Se-NPs demonstrated diminishing effects due to the downregulation of Smad1 and BMP2 genes, leading to impaired osteoblast differentiation. In the present work, it was observed that incorporating Se-NPs into a hydrogel matrix promoted osteoblast differentiation even at a higher concentration of Se-NPs, within the same time interval. Therefore, our synthesized materials may have an important role in the field of bone regeneration, with additional advantages of being biocompatible and having a bone mimicking polymeric matrix combined with Se-NPs. The encapsulation of Se-NPs within the hydrogels enhances the stability of the Se-NPs and protects them from uncontrolled degradation in the biological environment. This encapsulation also improves the bioavailability of the Se-NPs, ensuring more effective delivery to the target site or tissue. The prepared hydrogel matrix can be designed to respond to specific stimuli (such as pH, temperature), allowing for precise control over the release kinetics of any encapsulated drugs in future research.

5. Conclusion

This study successfully developed Se-NPs-functionalized hydrogels with advanced osteogenic capabilities. All the hydrogels were found to be thermoresponsive with a sol–gel transition occurring at the physiological temperature of 37 °C. CS and Coll were cross-linked with each other through β-GP and integrated with Se-NPs, which enhanced the crosslinking through Se–O covalent bonds and resulted in optimal thermoresponsive and injectability properties. The Se-NPs-integrated hydrogels were non-toxic and significantly increased cell proliferation and osteogenic differentiation compared to pure CS/Coll (S0) in both types of MSCs tested *in vitro*. We used rMSCs^{OVX} as a model to achieve efficient MSCs differentiation into osteoblasts with negligible cytotoxicity. Notably, the cell proliferation and osteogenic differentiation in rMSCs^{OVX} were found to be Se-NPs-concentration-dependent. Specifically, 2.56 mM Se-NPs treatment negatively affected the proliferation of rMSCs^{OVX}. Cell surface marker staining showed the potential of the prepared hydrogels for regeneration. We established a positive correlation between a higher CD73 expression with RUNX2 and increased calcium mineralization. Thus, taken together, our formulated hydrogels could be very promising as novel therapeutic biomaterials for repairing diseased bone.

To further validate the results, *in vivo* studies are necessary to understand the long-term effects and potential for clinical translation. Future research should also focus on elucidating the precise molecular mechanism for more targeting and efficient therapeutic strategies. The use of Se-NPs-loaded hydrogels in regenerating other types of tissues beyond bone, such as cartilage/muscle, could open a new research area for regenerative medicine. Se-NPs possess intrinsic anti-inflammatory and antioxidant properties, which can be beneficial for treating inflammatory diseases and reducing oxidative stress in various clinical conditions. These properties can enhance the therapeutic outcomes when used in drug-delivery systems.

9280 | *J. Mater. Chem. B*, 2024, **12**, 9268–9282

This journal is © The Royal Society of Chemistry 2024

Data availability

Data will be available on request.

Conflicts of interest

The authors declare no conflict of interest.

Acknowledgements

References

1 M. Ravi, V. Paramesh, S. R. Kaviya, E. Anuradha and F. D. Solomon, *J. Cell. Physiol.*, 2015, **230**, 16–26.

2 N. Annabi, A. Tamayol, J. A. Uquillas, M. Akbari, L. E. Bertassoni, C. Cha, G. Camci-Unal, M. R. Dokmeci, N. A. Peppas and A. Khademhosseini, *Adv. Mater.*, 2014, **26**, 85–123.

3 N. A. Peppas, J. Z. Hilt, A. Khademhosseini and R. Langer, *Adv. Mater.*, 2006, **18**, 1345–1360.

4 S. S. Liow, Q. Dou, D. Kai, A. A. Karim, K. Zhang, F. Xu and X. J. Loh, *ACS Biomater. Sci. Eng.*, 2016, **2**, 295–316.

5 Q. Q. Dou, S. S. Liow, E. Ye, R. Lakshminarayanan and X. J. Loh, *Adv. Healthcare Mater.*, 2014, **3**, 977–988.

6 A. Fabiano, R. Bizzarri and Y. Zambito, *Int. J. Nanomed.*, 2017, **12**, 633–643.

7 P. J. Kondiah, Y. E. Choonara, P. P. Kondiah, T. Marimuthu, P. Kumar, L. C. du Toit and V. Pillay, *Molecules*, 2016, **21**, 1580.

8 F. Ganji, M. J. Abdekhodaie and S. A. Ramazani, *J. Sol-Gel Sci. Technol.*, 2007, **42**, 47–53.

9 C. H. Lee, A. Singla and Y. Lee, *Int. J. Pharm.*, 2001, **221**, 1–22.

10 K. Kaur, S. S. Paiva, D. Caffrey, B. L. Cavanagh and C. M. Murphy, *Mater. Sci. Eng., C*, 2021, **128**, 112340.

11 W. Bao, M. Li, Y. Yang, Y. Wan, X. Wang, N. Bi and C. Li, *Front. Chem.*, 2020, **8**, 53.

12 B. Bellich, I. D'Agostino, S. Semeraro, A. Gamini and A. Cesàro, *Mar. Drugs*, 2016, **14**, 99.

13 A. H. Choi and B. Ben-Nissan, *Marine-derived biomaterials for tissue engineering applications*, Springer, 2019.

14 R. Sergi, D. Bellucci and V. Cannillo, *Materials*, 2020, **13**, 5560.

15 A. Ressler, A. Žužić, I. Ivanišević, N. Kamboj and H. Ivanković, *Open Ceram.*, 2021, **6**, 100122.

16 P. Sánchez-Cid, M. Jiménez-Rosado, J. F. Rubio-Valle, A. Romero, F. J. Ostos, M. Rafii-El-Idrissi Benhnia and V. Perez-Puyana, *Polymers*, 2022, **14**, 272.

17 H. Zhou, K. Yu, H. Jiang, R. Deng, L. Chu, Y. Cao, Y. Zheng, W. Lu, Z. Deng and B. Liang, *Biomacromolecules*, 2021, **22**, 4552–4568.

18 S. P. Zustiak, Y. Wei and J. B. Leach, *Tissue Eng., Part B*, 2013, **19**, 160–171.

19 B.-H. Shan and F.-G. Wu, *Adv. Mater.*, 2024, **36**, 2210707.

20 C. T. Laurencin, K. M. Ashe, N. Henry, H. M. Kan and K. W. H. Lo, *Drug Discovery Today*, 2014, **19**, 794–800.

21 T. Jung, J. H. Lee, S. Park, Y. J. Kim, J. Seo, H. E. Shim, K. S. Kim, H. S. Jang, H. M. Chung, S. G. Oh, S. H. Moon and S. W. Kang, *Stem Cells Int.*, 2017, **2017**, 1089–1098.

22 N. Sarin, M. Kurakula, K. J. Singh, A. Kumar, D. Singh and S. Arora, *J. Asian Ceram. Soc.*, 2021, **9**, 531–548.

23 C. García-Astrain, C. Chen, M. Burón, T. Palomares, A. Eceiza, L. Fruk, M. Corcuera and N. Gabilondo, *Biomacromolecules*, 2015, **16**, 1301–1310.

24 M. P. Rayman, *Lancet*, 2000, **356**, 233–241.

25 S. C. Lee, N. H. Lee, K. D. Patel, T. S. Jang, J. C. Knowles, H. W. Kim, H. H. Lee and J. H. Lee, *Nanomaterials*, 2021, **11**, 557.

26 N. d S. d Costa, L. S. Lima, M. E. A. Galiciolli, D. H. F. Ribeiro, M. M. Ribeiro, G. d P. J. Garica, I. S. Marçal, J. F. d Silva, M. E. Pereira, C. S. Oliveira and I. C. Guiloski, *J. Trace Elem. Med. Biol.*, 2024, **84**, 127446.

27 Q. Zhou, W. Chen, C. Gu, H. Liu, X. Hu, L. Deng, W. He, Y. Xu, X. Zhu, H. Yang, X. Chen, F. He and T. Liu, *Regener. Biomater.*, 2023, **10**, rbad011.

28 C. Liu, C. Wang, Y. Liu, J. Huang, W. Xu, J. Li, Y. Wang, Y. Xu, L. Zhu and H. Xu, *Int. J. Pharm.*, 2024, **653**, 123929.

29 W. Hu, X. Yao, Y. Li, J. Li, J. Zhang, Z. Zou, F. Kang and S. Dong, *Mater. Today Bio*, 2023, **23**, 100864.

30 K. K. Karthik, B. V. Cheriyan, S. Rajeshkumar and M. Gopalakrishnan, *Biomed. Technol.*, 2024, **6**, 61–74.

31 R. Xu, Y. You, W. Zheng, L. Ma, Y. Chang, S. Pan, Y. He, M. Zhou, Z. Xu, T. Chen and H. Liu, *Adv. Funct. Mater.*, 2024, **34**, 2313122.

32 S. Fatima, R. Alfrayh, M. Alrashed, S. Alsobaie, R. Ahmad and A. Mahmood, *Int. J. Nanomed.*, 2021, **16**, 331–343.

33 Q. Dang, K. Liu, Z. Zhang, C. Liu, X. Liu, Y. Xin, X. Cheng, T. Xu, D. Cha and B. Fan, *Carbohydr. Polym.*, 2017, **167**, 145–157.

34 L. Wang and J. P. Stegemann, *Biomaterials*, 2010, **31**, 3976–3985.

35 D. G. Menter, A. L. Sabichi and S. M. Lippman, *Cancer Epidemiol., Biomarkers Prev.*, 2000, **9**, 1171–1182.

36 M. Vahdati and T. Tohidi Moghadam, *Sci. Rep.*, 2020, **10**, 510.

37 J. Cho, M. C. Heuzey, A. Bégin and P. J. Carreau, *Biomacromolecules*, 2005, **6**, 3267–3275.

38 R. N. Power, B. L. Cavanagh, J. E. Dixon, C. M. Curtin and F. J. O'Brien, *Int. J. Mol. Sci.*, 2022, **23**, 1460.

39 E. G. Tierney, G. P. Duffy, A. J. Hibbitts, S.-A. Cryan and F. J. O'Brien, *J. Controlled Release*, 2012, **158**, 304–311.

40 P. Virtanen and K. Isotupa, *Acta Anat.*, 2008, **108**, 202–207.

This journal is © The Royal Society of Chemistry 2024

J. Mater. Chem. B, 2024, **12**, 9268–9282 | 9281

41 C. Payne, E. B. Dolan, J. O'Sullivan, S. A. Cryan and H. M. Kelly, *Drug Delivery Transl. Res.*, 2017, **7**, 132–146.

42 K. Kobayashi, C.-i Huang and T. P. Lodge, *Macromolecules*, 1999, **32**, 7070–7077.

43 B. El-Deeb, A. Al-Talhi, N. Mostafa and R. Abou-assy, *Am. J. Eng. Res.*, 2018, **45**, 135–170.

44 L. Fritea, V. Laslo, S. Cavalu, T. Costea and S. I. Vicas, *Studia Universitatis "Vasile Goldis" Arad. Seria Stiintele Vietii (Life Sciences Series)*, 2017, vol. 27, pp. 203–208.

45 M. H. Santos, R. M. Silva, V. C. Dumont, J. S. Neves, H. S. Mansur and L. G. Heneine, *Mater. Sci. Eng., C*, 2013, **33**, 790–800.

46 C. D. Moreira, S. M. Carvalho, H. S. Mansur and M. M. Pereira, *Mater. Sci. Eng., C*, 2016, **58**, 1207–1216.

47 K. Bai, B. Hong, Z. Hong, J. Sun and C. Wang, *J. Nanobiotechnol.*, 2017, **15**, 92.

48 M. G. Hassan, M. T. Hawwa, D. M. Baraka, H. M. El-Shora and A. A. Hamed, *BMC Microbiol.*, 2024, **24**, 21.

49 K. Kaur, K. J. Singh, V. Anand, G. Bhatia, R. Kaur, M. Kaur, L. Nim and D. S. Arora, *Mater. Sci. Eng., C*, 2017, **71**, 780–790.

50 A. Chenite, C. Chaput, D. Wang, C. Combes, M. D. Buschmann, C. D. Hoemann, J. C. Leroux, B. L. Atkinson, F. Binette and A. Selmani, *Biomaterials*, 2000, **21**, 2155–2161.

51 H. Y. Zhou, L. J. Jiang, P. P. Cao, J. B. Li and X. G. Chen, *Carbohydr. Polym.*, 2015, **117**, 524–536.

52 I.-K. Yoon, J.-Y. Hwang, J.-W. Seo, W.-C. Jang, H.-W. Kim and U. S. Shin, *Carbon*, 2014, **77**, 379–389.

53 S. Midha, S. Kumar, A. Sharma, K. Kaur, X. Shi, P. Naruphontjirakul, J. R. Jones and S. Ghosh, *Biomed. Mater.*, 2018, **13**, 055012.

54 C. García-Astrain, K. González, T. Gurrea, O. Guaresti, I. Algar, A. Eceiza and N. Gabilondo, *Carbohydr. Polym.*, 2016, **149**, 94–101.

55 S. Yasmeen, M. K. Kabiraz, B. Saha, M. Qadir, M. Gafur and S. Masum, *Int. Res. J. Pure Appl. Chem.*, 2016, **10**, 1–14.

56 M. Fernandes Queiroz, K. R. T. Melo, D. A. Sabry, G. L. Sassaki and H. A. O. Rocha, *Mar. Drugs*, 2015, **13**, 141–158.

57 S. Merino, C. Martín, K. Kostarelos, M. Prato and E. Vázquez, *ACS Nano*, 2015, **9**, 4686–4697.

58 J. C. Lassègues, J. Grondin, D. Cavagnat and P. Johansson, *J. Phys. Chem. A*, 2009, **113**, 6419–6421.

59 V. Anand, K. J. Singh, K. Kaur, H. Kaur and D. S. Arora, *Ceram. Int.*, 2016, **42**, 3638–3651.

60 T. T. Zhang, J. F. Jia and H. S. Wu, *J. Phys. Chem. A*, 2010, **114**, 12251–12257.

61 I. F. Amaral, R. E. Unger, S. Fuchs, A. M. Mendonça, S. R. Sousa, M. A. Barbosa, A. P. Pêgo and C. J. Kirkpatrick, *Biomaterials*, 2009, **30**, 5465–5475.

62 X. Tian, X. Yan, N. Zang, W. Duan, T. Wang, X. Li, L. Ma, L. Chen, J. Chen and X. Hou, *Mater. Today Bio*, 2024, **25**, 100967.

63 C. Liu and J. Sun, *Biomacromolecules*, 2014, **15**, 436–443.

64 J. Holinka, M. Pilz, B. Kubista, E. Presterl and R. Windhager, *Bone Joint J.*, 2013, **95B**, 678–682.

65 C. M. Murphy, M. G. Haugh and F. J. O'Brien, *Biomaterials*, 2010, **31**, 461–466.

66 C. Zheng, J. Wang, Y. Liu, Q. Yu, Y. Liu, N. Deng and J. Liu, *Adv. Funct. Mater.*, 2014, **24**, 6872–6883.

67 D. Sun, Y. Liu, Q. Yu, Y. Zhou, R. Zhang, X. Chen, A. Hong and J. Liu, *Biomaterials*, 2013, **34**, 171–180.

68 L. Zeng, P. Gupta, Y. Chen, E. Wang, L. Ji, H. Chao and Z. S. Chen, *Chem. Soc. Rev.*, 2017, **46**, 5771–5804.

69 V. Diwadkar-Navsariwala, G. S. Prins, S. M. Swanson, L. A. Birch, V. H. Ray, S. Hedayat, D. L. Lantvit and A. M. Diamond, *Proc. Natl. Acad. Sci. U. S. A.*, 2006, **103**, 8179–8184.

70 J. Hou, Y. Tamura, H. Y. Lu, Y. Takahashi, S. Kasugai, H. Nakata and S. Kuroda, *Nanomaterials*, 2022, **12**, 1850.

71 J. Goergen, S. Wenisch, O. Raabe, A. Moritz, G. Schlewitz, R. Schnettler, U. Hempel, C. Heiss and S. Arnhold, *ISRN Stem Cells*, 2013, **2013**, 262451.

72 J. P. Rodríguez, L. Montecinos, S. Ríos, P. Reyes and J. Martínez, *J. Cell. Biochem.*, 2000, **79**, 557–565.

73 J. P. Rodríguez, S. Garat, H. Gajardo, A. M. Pino and G. Seitz, *J. Cell. Biochem.*, 1999, **75**, 414–423.

74 S. Kawre, P. Suryavanshi, D. S. Lalchandani, M. K. Deka, P. Kumar Porwal, S. Kaity, S. Roy and S. Banerjee, *Eur. Polym. J.*, 2024, **204**, 112702.

75 K. Kimura, M. Breitbach, F. A. Schildberg, M. Hesse and B. K. Fleischmann, *Bone Rep.*, 2021, **15**, 101133.

76 K. Tan, H. Zhu, J. Zhang, W. Ouyang, J. Tang, Y. Zhang, L. Qiu, X. Liu, Z. Ding and X. Deng, *Stem Cells Int.*, 2019, **2019**, 8717694.

9282 | *J. Mater. Chem. B*, 2024, **12**, 9268–9282

This journal is © The Royal Society of Chemistry 2024